The Influence of Carbon Quantum Dots Addition on the Photoluminescence Performance of ZnO Nanoparticles

Astuti*, S.R.A. Usna

Physics Department. Andalas University. Padang. West Sumatera. Indonesia (+6285263301026)
*astuti@sci.unand.ac.id
srirahayualfitri@sci.unand.ac.id

Abstract. Extensive exploration of ZnO luminous material for biomedical applications has been conducted in recent years due to its biocompatibility and optical characteristics that can be customized to meet specific needs. The ZnO was modified with carbon quantum dot (CQD) to produce a ZnO@COD composite with enhanced photoluminescence and to obtain ZnO luminescence to be used as a bioimaging material. The hydrothermal process was adopted to produce ZnO nanoparticles. The modification of ZnO with carbon quantum dots was performed via a simple method of stirring and sonication. The effects of variations in the amount of carbon dots on the optical properties of ZnO@CQD nanocomposites were investigated. The optical properties of ZnO@CQD were characterized using UV-Vis and photoluminescence spectroscopy. The UV-Vis spectra revealed a decrease in the gap energy of ZnO@CQD. Additionally, the photoluminescence spectroscopy showed a significant increase in photoluminescence intensity with the addition of 10 ml of carbon dots. There was also a redshift of the photoluminescence band to the long-wavelength region. The optical properties of the ZnO@CQD nanocomposites discovered in this study demonstrate their potential use as bioimaging materials in biomedical applications.

Keywords: magnetic, bioimaging, luminescence, nanocomposites

1. Introduction

The demand for biocompatible and environmentally friendly nanomaterials has continued to grow each year. The need is particularly significant for photocatalysts [1–3], biomedical [4,5], and other applications. The use of nanomaterials in the biomedical field has rapidly developed, which includes materials for diagnosis, treatment, and therapy. The application of imaging techniques for the diagnosis of diseases has particularly garnered significant interest among researchers. Biological imaging technology employs various strategies to analyze and solve the

mysteries of the human body, understand the roots of disease, and develop individualized or personalized treatment. The performance of the bioimaging techniques relies on the use of probes with high specificity and sensitivity. Therefore, exploring materials with excellent photoluminescence properties and employing suitable strategies for their synthesis and application is necessary to analyze the biological microenvironment and related processes [6–8]. Despite the growing proposal of new imaging strategies in recent studies, further development of phosphors with enhanced brightness and luminous properties is required. In addition, the recent advances in clinical technology and instruments for photoluminescence imaging induction surgery in patients have led to the demand for further development of photoluminescence [9–11].

Photoluminescence imaging technology offers advantages for biomedical imaging applications, which include high sensitivity, low cost, and high spatial/temporal resolution. The use of materials such as nanocarbon [12,13], semiconductor quantum dots (QDs) [14], and rare earth-doped nanoparticles [15] as fluorescent probes have been reported in several studies. However, these probes have limitations that include low quantum yield, low solubility, high cytotoxicity, and low photostability. The use of Zinc oxide (ZnO) has garnered considerable interest due to its high photoluminescence in visible regions, low cost, and biocompatibility [16–20]. The use of ZnO nanoparticles as photocatalysts [21–26], anti-bacterial agents [27], sensor components [28,29], drug delivery agents [30], and others have been reported in recent studies. Although ZnO exhibits considerably enhanced photoluminescence in the visible light area, the resulting photoluminescence is unstable due to defects, such as vacancies and interstitial and dangling bonds on the ZnO surface [18,20,21]. Therefore, it is necessary to modify the ZnO surface with other materials to improve its photoluminescence properties.

One material with the potential for hybridization with ZnO is carbon quantum dot (CQD). CQDs have received substantial attention because of their properties, including non-toxic, photostable, low-cost, heavy metal-free, and eco-friendly [31–33]. The application of CQDs has been acknowledged due to the characteristic photo-induced electron transfer [34,35] and up-conversion of photoluminescence properties [36]. CQD is synthesized from dried banana leaves using the hydrothermal method. The application of green chemistry in the synthesis process is fundamental for biomaterial development to produce non-toxic materials that are environmentally friendly and safe for human use [10,14,37]. However, the hybridization of ZnO and CQD for bioimaging applications is still limited. In this study, the ZnO surface was modified

using CQDs via sonication technique to increase the intensity and stability of ZnO photoluminescence. A volume of 10 mL of CQD could significantly increase the photoluminescence of ZnO@CQD. However, adding more CQDs could cause a quenching effect on their photoluminescence. This article reports in detail the influence of the amount of CQD on the structure and optical properties of ZnO@CQD.

2. Methods

2.1 Materials

ZnO@CQD nanocomposites were synthesized using the following materials: sodium hydroxide (NaOH, Bratachem), zinc nitrate ($Zn(NO_3)_2.6H_2O$, Merck). The synthesized nanocomposites were characterized using an X-ray diffractometer (XRD) (Bruker D8 Advance), photoluminescence (PL) (Horiba MicrO Photoluminescence Microspectrometer), scanning electron microscopy (SEM) (SEM, Zeiss, EVO 15), and Fourier transform infrared spectroscopy (FTIR) (FTIR, Nicolet iS50).

2.2 Experiment

2.2.1 Synthesis ZnO

The hydrothermal process was adopted for the synthesis of ZnO. The ZnO was prepared by mixing $Zn(NO_3)_2.6H_2O$ and NaOH at a molar mass ratio of 1:2. $Zn(NO_3)_2.6H_2O$ of 0.5 M and 1 M NaOH was dissolved in 50 ml and 10 ml of distilled water, respectively. The $Zn(NO_3)_2.6H_2O$ solution was stirred using a magnetic stirrer with a rotational speed of 300 rpm, with a gradual addition of NaOH solution using a dropper until a pH of 11 was achieved. The sample was autoclaved at 180 °C for three hours in an oven. Next, the sample was filtered and washed twice with alcohol and distilled water. Then, the sample was put into the furnace and heated at 200 °C for 12 hours. The sample was crushed to obtain ZnO powder, which was subsequently used for structural and optical analysis.

2.2.2 Synthesis of CQD

CQD synthesis was achieved via the hydrothermal process. Banana leaves were dried in a furnace at 200 °C for one hour. At this temperature, the celluloses in dried banana leaves start to decompose [38]. Next, the dried banana leaves were crushed and filtered using a 300-mesh sieve.

The carbonization process was carried out at 400 °C for one hour in a furnace. Subsequently, 0.5 g of carbon powder was dissolved in 50 ml of distilled water and transferred to an autoclave oven to initiate the hydrothermal process at 180 °C for 12 hours.

2.2.3 Synthesis of ZnO@CQD

The synthesis of ZnO@CQD was carried out by dissolving 0.3 g of ZnO powder in 5 ml of CQD colloid. The solution was subsequently sonicated for 90 minutes. Next, the solution was heated in an oven at 180 °C for 15 hours. The precipitate was crushed using a mortar and pestle to obtain ZnO@CQD powder. All these steps were repeated using a volume of 10 and 20 ml of CQD colloid.

3. Results and Discussion

3.1 XRD and SEM Analysis

The XRD diffraction patterns of ZnO and ZnO/CQD (5 mL) are shown in Figure 1 (a). The XRD analysis of ZnO revealed diffraction peaks that match the ICDD data reference code 01-073-8765. The highest peak was identified at angle $2\theta = 36.23^{o}$ with the Miller index (101). The crystal structure of ZnO appeared as hexagonal wurtzite with lattice parameters of $a = b = 3.25$ Å and $c = 5.20$ Å. The ZnO@CQD nanocomposite exhibited ZnO and C (CQD) diffraction peaks, with the highest peak at an angle of $2\theta = 36.21^{o}$, identified as ZnO. The results indicate the absence of peaks that correspond to possible impurities. The crystal structure of ZnO appeared as a hexagonal wurtzite with lattice parameters of $a = b = 3.25$ Å and $c = 5.20$ Å. The presence of CQD in the sample is evidenced by carbon diffraction peaks at $2\theta = 23.55^{o}$ and $2\theta = 41.16^{o}$, which correspond to the Miller indices (002) and (440), respectively. ICDD data with reference code 00-049-1717 shows a cubic crystal structure of phase C with lattice parameters of $a = b = c = 12.38$ Å, which corresponds to the sp^2 graphite crystal of the graphene phase. The *d*-spacing of CQD is 3.77 Å, which is slightly larger than the *d*-spacing of graphite (3.4 Å). This increase in the interlayer distance value was likely caused by the presence of oxygen on the CQD surface [39]. The crystal size of ZnO nanoparticles and ZnO@CQD nanocomposites was determined using the Debye-Scherrer equation.

$$D = \frac{K\lambda}{\beta \cos\theta} \quad (1)$$

In eq. (1), D is the nanoparticle crystalline size, K represents the Scherrer constant (0.98), λ denotes the wavelength (1.54 Å), and β denotes the full width at half maximum (FWHM).
The crystal size of ZnO nanoparticles was 27.27 nm, while the ZnO@CQD nanocomposite was 40.86 nm. The results also indicate an increase in crystal size with the addition of CQD to ZnO nanoparticles. The XRD data reveals that the increase in crystal size was also accompanied by an increase in *d*-spacing, i.e., 2.47919 Å (ZnO) to 2.48039 Å (ZnO@CQD).

The morphology and particle size of ZnO@CQD are presented in Figure 2 (b). The particles appeared spherical, with a diameter of 20–50 nm. The particle size appeared relatively homogeneous, with an average size of 42.5 nm.

3.2 FTIR Analysis

The profiles of ZnO@CQD nanocomposites with CQD variations of 10 ml and 20 ml were generated via FTIR analysis. This characterization aimed to investigate the molecular groups contained in the nanocomposite at wavenumbers of 400 cm^{-1} to 4500 cm^{-1}. The FTIR profile is shown in Figure 3.
Figure 3 shows the similarities in the absorption peaks in the two samples and their differences—the higher the CQD colloid volume, the weaker the absorption. In general, the O-H (hydroxyl) group with wavenumbers 3338.78 cm^{-1}-3392.79 cm^{-1} was present in all samples. This absorption peak indicates the presence of water as a solvent. The wavenumbers of 1348.24 cm^{-1} represent the C-H functional group bond, whereas the wavenumbers of 1583.56 cm^{-1}-1631.78 cm^{-1} indicate the C=C functional group and the wavenumbers of 1764.87 cm^{-1}-1934.60 cm^{-1} indicates the C=O bond. These peaks indicate the formation of CQD, as C=C is the main functional group in CQD [40,41] Meanwhile, the absorption peak at wavenumbers of 476.42 cm^{-1}-526.57 cm^{-1} indicates the formation of Zn-O bonds.

3.3 UV-Vis and Photoluminescence Analysis

The optical characteristics of ZnO and ZnO@CQD were determined using UV-Vis and photoluminescence spectroscopy. The results from the UV-Vis analysis are presented in Figure 4. Figure 4 (a) shows the absorption spectrum of ZnO and ZnO@CQD against wavelength and Figure 4 (b) shows the gap energy of ZnO and ZnO@CQD.

Figure 4 (a) depicts the higher absorption of ZnO@CQD than ZnO. The absorption peak of ZnO@CQD increased as the energy gap decreased, as proven by the application of the Kubelka−Munk function from the Tauc plot method presented in Figure 4(b). The energy gap value for ZnO and ZnO@CQD was 3.39 eV and 3.34 eV, respectively. The results demonstrate a slight decrease in the energy gap due to the presence of CQD.

The photoluminescence spectra of ZnO and ZnO@CQD nanocomposites are shown in Figure 5. There are two emission bands: The first band is a narrow UV emission band (λ = 360 nm for ZnO and λ = 370 nm for ZnO@CQD). The UV emission peak denotes the optical activity of the intrinsic defects of ZnO, which resulted in near-band edge (NBE) excitons. The second band is the visible light emission peak (λ = 500–760 nm), which corresponds to deep-level defects (DLE) in ZnO. The synthesis process, morphology, vacancies, and surface defects influence luminescence emission in the visible light region. In UV emission (NBE), ZnO nanoparticles can only absorb light of less than 400 nm, indicating a response range that is concentrated in the UV region.

Additionally, the ZnO@CQD composite exhibited a continuous absorption edge in the visible light region, suggesting the ability of CQD to extend the light response to the visible light region, thereby absorbing more photons. CQD did not only absorb visible light but also demonstrated an up-conversion luminescence, resulting in a higher absorption by the CQD@ZnO composite. Similar photoluminescence curves were observed for ZnO nanoparticles and ZnO@CQD nanocomposites, indicating that CQD modification does not produce new photoluminescence responses and characteristics. Nevertheless, an increase in intensity and a shift in the emission region occurred as a result of the modification.

The addition of CQD to ZnO caused a significant increase in photoluminescence intensity, particularly in the visible light region. The change is caused by the rapid recombination of electrons and holes between ZnO and CQD. The highest photoluminescence intensity was obtained from the ZnO@CQD sample (10 mL), while the lowest intensity was obtained from the ZnO@CQD sample (5 mL). However, adding more CQD to ZnO@CQD (20 mL) reduced the photoluminescence intensity due to the quenching effect in the presence of excess CQD. Excessive amount of CQD causes internal absorption in the CQD [42,43]. Other studies have attributed the quenching effect in the presence of excess CQD to the lack of dispersion and formation of CQD aggregates, thereby reducing contact between ZnO and the CQD [44,45].

Besides, CQD also triggers a shift in the emission band at longer wavelengths. ZnO produces yellow photoluminescence, while the addition of CQD produces orange photoluminescence. The photoluminescence mechanism of ZnO and ZnO@CQD is shown in Figure 6.

Figure 6 (a) shows the photoluminescence spectrum of ZnO and ZnO@CQD (10 mL) and Figure 6 (b) shows the difference in optical transition between ZnO and ZnO@CQD. There was a change in electron transition energy from the donor to the acceptor level, such as purple emission (NBE), which is a transition from the edge of the conduction band at the exciton binding energy level, i.e., from 0.06 eV below the conduction band to the valence band with an energy of 3.33 eV in ZnO and 3.28 eV in ZnO@CQD. The yellow emission (2.1 eV) was caused by the electron transition from Zn_i to the oxygen vacancy state (V_O) [46,47]. In ZnO@CQD, there was a shift from yellow emission to orange emission (1.9 eV), which was caused by the transition of electrons from interstitial Zn (Zn_i) to interstitial oxygen (O_i), which is translated as a decrease in the transition energy by ~ 0.2 eV. The results from photoluminescence analysis demonstrate that the addition of CQD causes a decrease in the amount of V_O and an increase in the amount of O_i in ZnO. In addition, the increase in intensity and shift of the photoluminescence band at longer wavelengths (orange) in the ZnO@CQD nanocomposite may also be caused by plasmon resonance on the CQD surface [48,49].

Conclusion

In this research, a ZnO@CQD luminescent nanocomposite material was developed. The analysis results from XRD, SEM, FTIR, and optical characterization confirm the successful synthesis of ZnO@CQD nanocomposites via the hydrothermal process. The XRD results show the formation of ZnO and ZnO@CQD phases with no impurity phases present. Additionally, ZnO nanoparticles produced yellow emissions in the visible light wavelength region, and the coupling of ZnO with varied amounts of CQD significantly increased the photoluminescence intensity. Besides increasing the intensity of photoluminescence, the presence of CQD in the ZnO@CQD nanocomposite also caused a shift in the emission band to the long wavelength region, namely orange emission. The optical properties of ZnO@CQD demonstrate its potential use in biomedical applications, particularly as bioimaging material.

Acknowledgments

The research described in this paper was financially supported by Universitas Andalas with research contract number No:14/UN.16.03.D/PP/FMIPA/2023.

References

1. Hua, J., Wang, Z., Zhang, J., et al. "A hierarchical Bi-MOF-derived BiOBr/Mn0.2Cd0.8S S-scheme for visible-light-driven photocatalytic CO2 reduction", *Journal of Materials Science & Technology*, **156**, pp. 64–71 (2023).
2. Panahi, A., Monsef, R., Dawi, E. A., et al. "Green auto-combustion synthesis and characterization of TmVO4 nanostructures in the presence carbohydrate sugars and their application as Visible-light photocatalyst", *Solar Energy*, **258**, pp. 372–382 (2023).
3. Zhao, Z., Wang, Z., Zhang, J., et al. "Interfacial Chemical Bond and Oxygen Vacancy-Enhanced In $_2$ O $_3$ /CdSe- DETA S- scheme Heterojunction for Photocatalytic CO $_2$ Conversion", *Adv Funct Materials*, **33**(23), p. 2214470 (2023).
4. Khosravanian, A., Moslehipour, A., and Ashrafian, H. "A review on Bioimaging, Biosensing, and Drug Delivery Systems Based on Graphene Quantum Dots", *Prog. Chem. Biochem. Res.*, (Online First) (2020).
5. Liu, J., Kotrchová, L., Lécuyer, T., et al. "Coating Persistent Luminescence Nanoparticles With Hydrophilic Polymers for in vivo Imaging", *Front. Chem.*, **8**, p. 584114 (2020).
6. Liu, F., Mou, X., Song, J., et al. "Novel Carbon-Based Magnetic Luminescent Nanocomposites for Multimodal Imaging", *Front. Chem.*, **8**, p. 611 (2020).
7. Perelshtein, I., Perkas, N., Rahimipour, S., et al. "Bifunctional Carbon Dots—Magnetic and Fluorescent Hybrid Nanoparticles for Diagnostic Applications", *Nanomaterials*, **10**(7), p. 1384 (2020).
8. Sk, M. P. and Dutta, A. "New-generation quantum dots as contrast agent in imaging", In *Nanomaterials in Diagnostic Tools and Devices*, Elsevier, pp. 525–556 (2020).
9. Jia, Z. and Misra, R. D. K. "Tunable ZnO quantum dots for bioimaging: synthesis and photoluminescence", *Materials Technology*, **28**(4), pp. 221–227 (2013).
10. Gupta, J., Hassan, P. A., and Barick, K. C. "Core-shell Fe $_3$ O $_4$ @ZnO nanoparticles for magnetic hyperthermia and bio-imaging applications", *AIP Advances*, **11**(2), p. 025207 (2021).
11. Rissi, N. C., Hammer, P., and Chiavacci, L. A. "Surface modification of ZnO quantum dots by organosilanes and oleic acid with enhanced luminescence for potential biological application", *Mater. Res. Express*, **4**(1), p. 015027 (2017).
12. Li, H., Kang, Z., Liu, Y., et al. "Carbon nanodots: synthesis, properties and applications", *J. Mater. Chem.*, **22**(46), p. 24230 (2012).
13. Park, Y. R., Liu, N., and Lee, C. J. "Photoluminescence enhancement from hybrid structures of metallic single-walled carbon nanotube/ZnO films", *Current Applied Physics*, **13**(9), pp. 2026–2032 (2013).
14. Wu, Y. L., Lim, C. S., Fu, S., et al. "Surface modifications of ZnO quantum dots for bio-imaging", *Nanotechnology*, **18**(21), p. 215604 (2007).
15. Min, Y., Li, J., Liu, F., et al. "Recent Advance of Biological Molecular Imaging Based on Lanthanide-Doped Upconversion-Luminescent Nanomaterials", *Nanomaterials*, **4**(1), pp. 129–154 (2014).

16. Mu, J., Shao, C., Guo, Z., et al. “High Photocatalytic Activity of ZnO−Carbon Nanofiber Heteroarchitectures”, *ACS Appl. Mater. Interfaces*, **3**(2), pp. 590–596 (2011).
17. Muthulingam, S., Bae, K. B., Khan, R., et al. “Improved daylight-induced photocatalytic performance and suppressed photocorrosion of N-doped ZnO decorated with carbon quantum dots”, *RSC Adv.*, **5**(57), pp. 46247–46251 (2015).
18. Li, Y., Zhang, B.-P., Zhao, J.-X., et al. “ZnO/carbon quantum dots heterostructure with enhanced photocatalytic properties”, *Applied Surface Science*, **279**, pp. 367–373 (2013).
19. Bozetine, H., Meziane, S., Aziri, S., et al. “Facile and green synthesis of a ZnO/CQDs/AgNPs ternary heterostructure photocatalyst: study of the methylene blue dye photodegradation”, *Bull Mater Sci*, **44**(1), p. 64 (2021).
20. Dai, K., Dawson, G., Yang, S., et al. “Large scale preparing carbon nanotube/zinc oxide hybrid and its application for highly reusable photocatalyst”, *Chemical Engineering Journal*, **191**, pp. 571–578 (2012).
21. Chua, S. T., Lim, K. Y., Zhang, Z., et al. “Selective micro laser annealing for fluorescence tuning of carbon-incorporated zinc oxide nanowire arrays”, *J. Mater. Chem. C*, **7**(21), pp. 6279–6288 (2019).
22. EL-Dafrawy, S. M., Tarek, M., Samra, S., et al. “Synthesis, photocatalytic and antidiabetic properties of ZnO/PVA nanoparticles”, *Sci Rep*, **11**(1), p. 11404 (2021).
23. Velumani, A., Sengodan, P., Arumugam, P., et al. “Carbon quantum dots supported ZnO sphere based photocatalyst for dye degradation application”, *Current Applied Physics*, **20**(10), pp. 1176–1184 (2020).
24. Mandal, S. K., Paul, S., Datta, S., et al. “Nitrogenated CQD decorated ZnO nanorods towards rapid photodegradation of rhodamine B: A combined experimental and theoretical approach”, *Applied Surface Science*, **563**, p. 150315 (2021).
25. Xu, J.-J., Lu, Y.-N., Tao, F.-F., et al. “ZnO Nanoparticles Modified by Carbon Quantum Dots for the Photocatalytic Removal of Synthetic Pigment Pollutants”, *ACS Omega*, **8**(8), pp. 7845–7857 (2023).
26. Liang, H., Tai, X., Du, Z., et al. “Enhanced photocatalytic activity of ZnO sensitized by carbon quantum dots and application in phenol wastewater”, *Optical Materials*, **100**, p. 109674 (2020).
27. Gao, D., Zhao, P., Lyu, B., Li, Y., et al. “Carbon quantum dots decorated on ZnO nanoparticles: An efficient visible- light responsive antibacterial agents”, *Appl Organomet Chem*, **34**(8) (2020).
28. Gaidi, M., Salem, M., Akir, S., et al. “ZnO and carbon nanocomposites for enhanced photoelectrochemical sensing activity: influence of the carbon content”, *J Solid State Electrochem*, **22**(11), pp. 3631–3637 (2018).
29. Jana, J., Chung, J. S., and Hur, S. H. “ZnO-Associated Carbon Dot-Based Fluorescent Assay for Sensitive and Selective Dopamine Detection”, *ACS Omega*, **4**(16), pp. 17031–17038 (2019).
30. Prasanna, A. P. S., Venkataprasanna, K. S., Pannerselvam, B., et al. “Multifunctional ZnO/SiO2 Core/Shell Nanoparticles for Bioimaging and Drug Delivery Application”, *J Fluoresc*, **30**(5), pp. 1075–1083 (2020).
31. Wang, Y. and Hu, A. “Carbon quantum dots: synthesis, properties and applications”, *J. Mater. Chem. C*, **2**(34), p. 6921 (2014).
32. Gao, X., Du, C., Zhuang, Z., et al. “Carbon quantum dot-based nanoprobes for metal ion detection”, *J. Mater. Chem. C*, **4**(29), pp. 6927–6945 (2016).

33. Teymourinia, H., Salavati-Niasari, M., Amiri, O., et al. “Synthesis of graphene quantum dots from corn powder and their application in reduce charge recombination and increase free charge carriers”, *Journal of Molecular Liquids*, **242**, pp. 447–455 (2017).
34. Safardoust-Hojaghan, H., Salavati-Niasari, M., Amiri, O., et al. “Preparation of highly luminescent nitrogen doped graphene quantum dots and their application as a probe for detection of Staphylococcus aureus and E. coli”, *Journal of Molecular Liquids*, **241**, pp. 1114–1119 (2017).
35. Wang, X., Cao, L., Lu, F., et al. “Photoinduced electron transfers with carbon dots”, *Chem Commun (Camb)*, (25), pp. 3774–3776 (2009).
36. Magesh, V., Sundramoorthy, A. K., and Ganapathy, D. “Recent Advances on Synthesis and Potential Applications of Carbon Quantum Dots”, *Front. Mater.*, **9**, p. 906838 (2022).
37. Zinatloo-Ajabshir, S., Baladi, M., and Salavati-Niasari, M. “Enhanced visible-light-driven photocatalytic performance for degradation of organic contaminants using PbWO4 nanostructure fabricated by a new, simple and green sonochemical approach”, *Ultrasonics Sonochemistry*, **72**, p. 105420 (2021).
38. Gagić, T., Perva-Uzunalić, A., Knez, Ž., et al. “Hydrothermal Degradation of Cellulose at Temperature from 200 to 300 °C”, *Ind. Eng. Chem. Res.*, **57**(18), pp. 6576–6584 (2018).
39. Yin, B., Deng, J., Peng, X., et al. “Green synthesis of carbon dots with down- and up-conversion fluorescent properties for sensitive detection of hypochlorite with a dual-readout assay”, *Analyst*, **138**(21), p. 6551 (2013).
40. Souza da Costa, R., Ferreira da Cunha, W., Simenremis Pereira, N., et al. “An Alternative Route to Obtain Carbon Quantum Dots from Photoluminescent Materials in Peat”, *Materials*, **11**(9), p. 1492 (2018).
41. Wanas, W., Abd El-Kaream, S. A., Ebrahim, S., et al. “Cancer bioimaging using dual mode luminescence of graphene/FA-ZnO nanocomposite based on novel green technique”, *Sci Rep*, **13**(1), p. 27 (2023).
42. Alarfaj, N., El-Tohamy, M., and Oraby, H. “CA 19-9 Pancreatic Tumor Marker Fluorescence Immunosensing Detection via Immobilized Carbon Quantum Dots Conjugated Gold Nanocomposite”, *IJMS*, **19**(4), p. 1162 (2018).
43. Rauwel, P., Salumaa, M., Aasna, A., et al. “A Review of the Synthesis and Photoluminescence Properties of Hybrid ZnO and Carbon Nanomaterials”, *Journal of Nanomaterials*, **2016**, pp. 1–12 (2016).
44. Suzuki, K., Nabata, H., Ueno, S., et al. “Origin of carbon dot fluorescence in organosilica films explored experimentally by surface functionalization”, *J Sol-Gel Sci Technol*, **104**(3), pp. 702–710 (2022).
45. Pérez-Cuapio, R., Alvarado, J. A., Pacio, M., et al. “Enhanced green photoluminescence and dispersion of ZnO quantum dots shelled by a silica shell”, *J Nanopart Res*, **22**(9), p. 254 (2020).
46. He, L., Mei, S., Chen, Q., et al. “Two-step synthesis of highly emissive C/ZnO hybridized quantum dots with a broad visible photoluminescence”, *Applied Surface Science*, **364**, pp. 710–717 (2016).
47. Manikandan, A., Yogasundari, M., Thanrasu, K., et al. “Structural, morphological and optical properties of multifunctional magnetic-luminescent ZnO@Fe3O4 nanocomposite”, *Physica E: Low-dimensional Systems and Nanostructures*, **124**, p. 114291 (2020).

48. Ko, Y. H., Kim, M. S., and Yu, J. S. “Structural and optical properties of ZnO nanorods by electrochemical growth using multi-walled carbon nanotube-composed seed layers”, *Nanoscale Res Lett*, **7**(1), p. 13 (2012).
49. Guo, D.-Y., Shan, C.-X., Liu, K.-K., et al. “Surface plasmon effect of carbon nanodots”, *Nanoscale*, **7**(45), pp. 18908–18913 (2015).

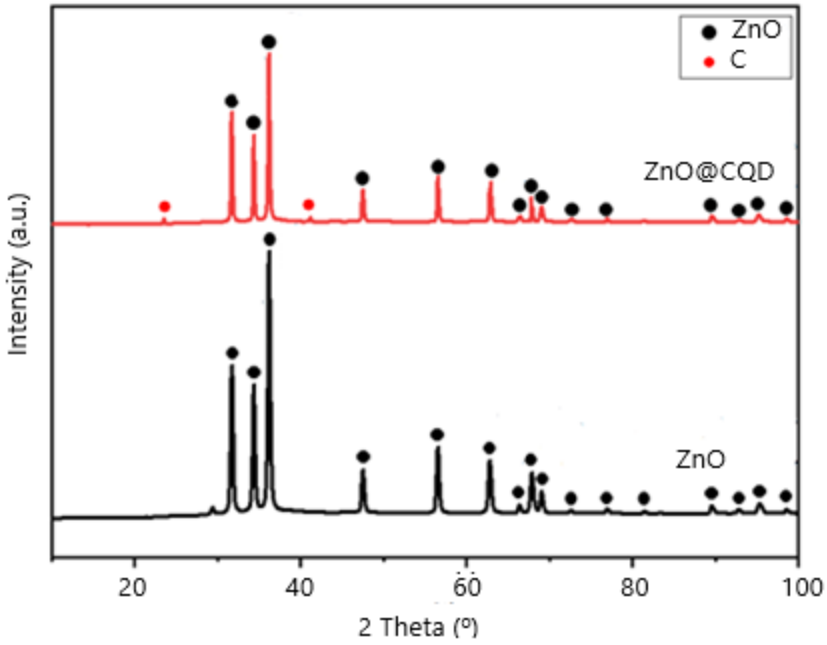

Figure 1. (a) XRD pattern of ZnO and ZnO@CQD

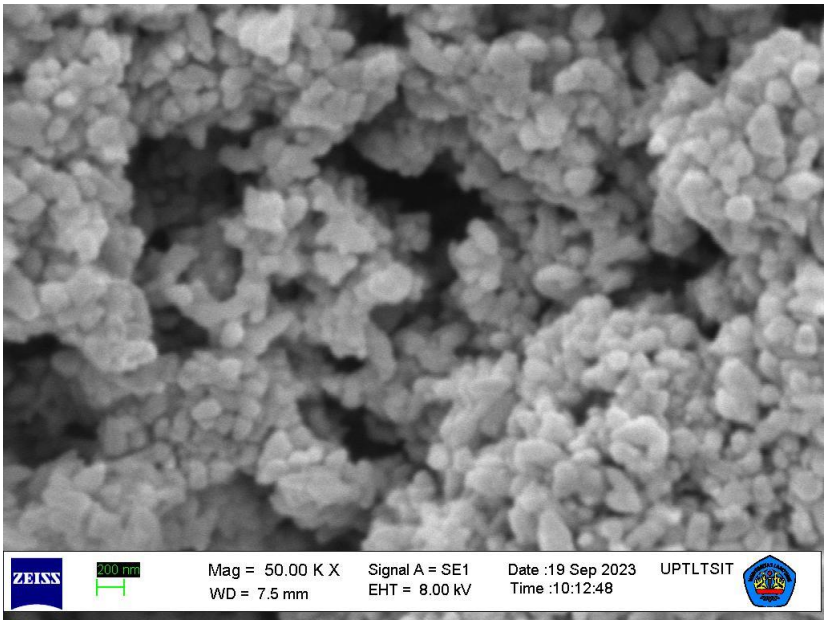

Figure 2. SEM image of ZnO@CQD

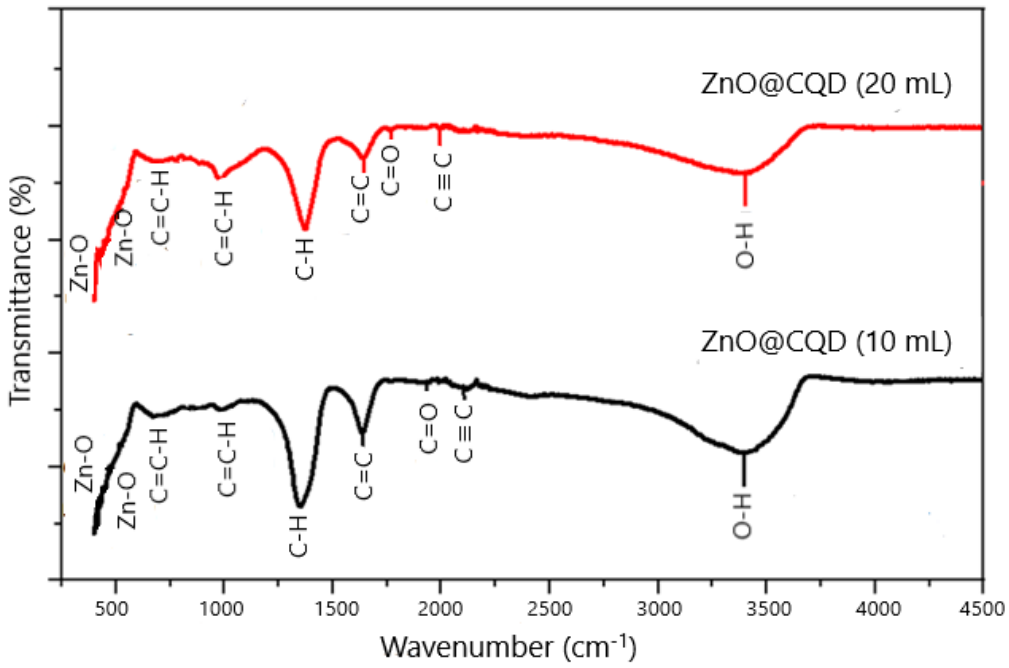

Figure 3. FTIR spectra of ZnO@CQD nanocomposites

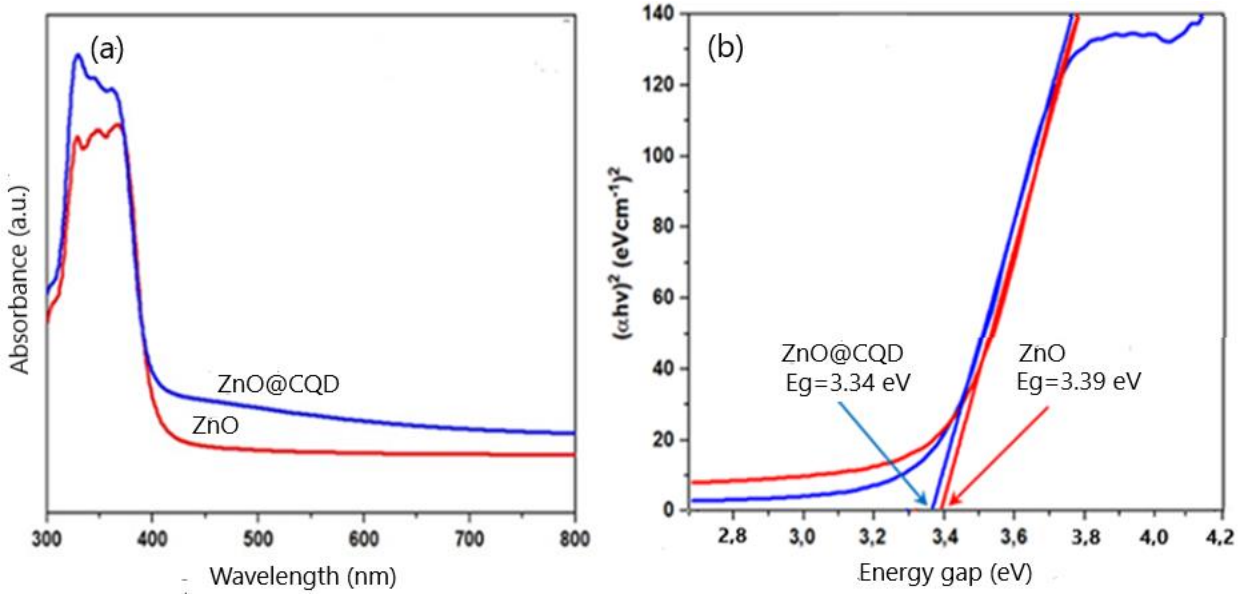

Figure 4. (a) UV-Vis absorption of ZnO and ZnO@CQD and (b) the energy gap in ZnO and ZnO@CQD.

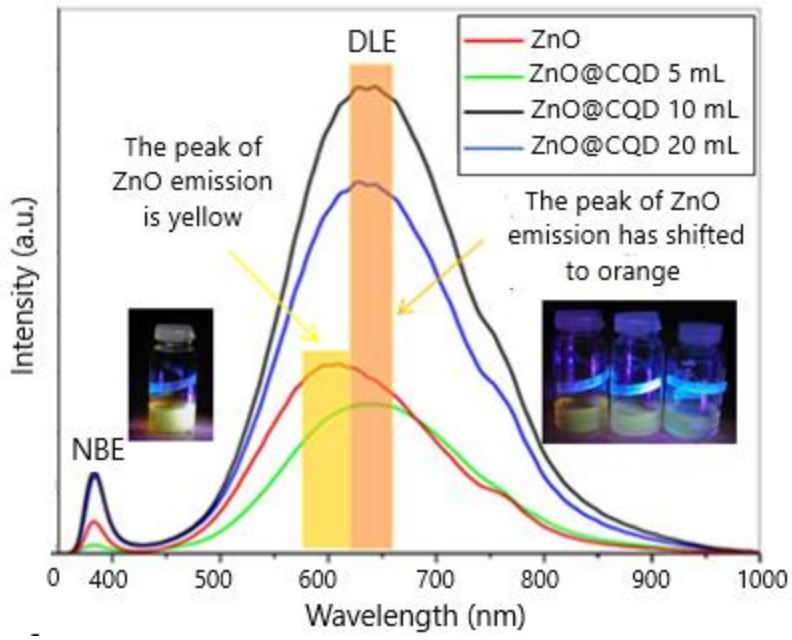

Figure 5. Photoluminescence spectrum on ZnO and ZnO@CQD.

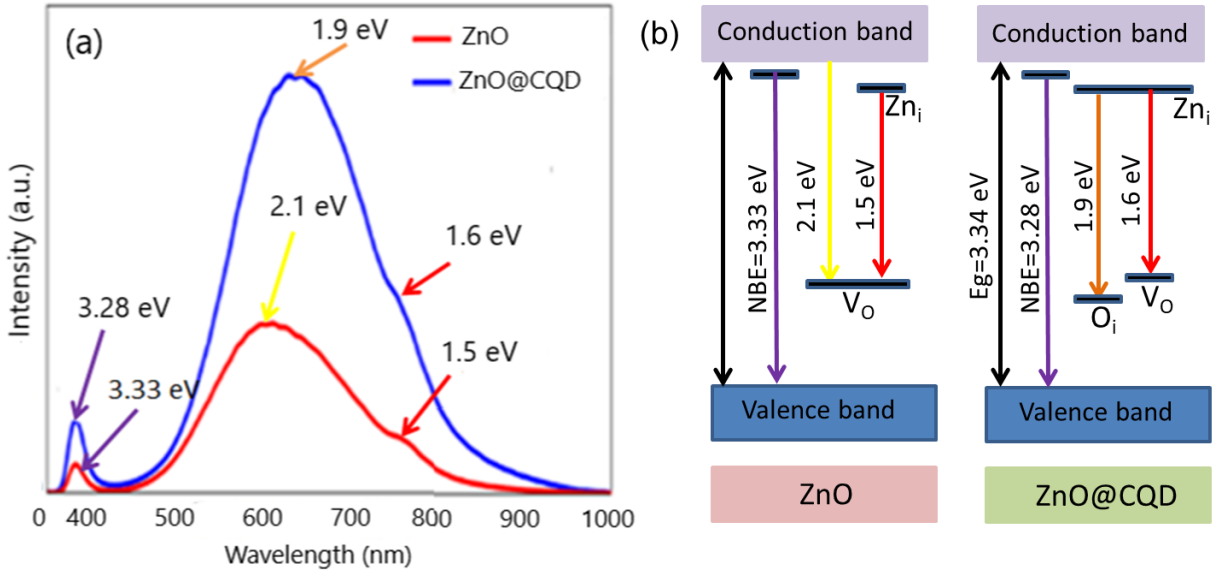

Figure 6. (a) Photoluminescence spectrum of ZnO and ZnO@CQD, (b) Band structure diagram of ZnO and ZnO@CQD obtained based on photoluminescence results.

Astuti is currently an Associate Professor at the Department of Physics at Andalas Universiti in Indonesia. She obtained her PhD degree in Chemistry at Andalas University (2023). She

obtained her BSc degree from Padang State University and MSc degrees from Bandung Insitute of Technology in Indonesia. Both BSc and MSc degrees are in Physics. Her research interest is the development of magnetic materials and luminescent materials in biomedical applications. She has written numerous articles in credible journals in these fields and has participated in many conferences

Sri Rahayu Alfitri Usna is currently an lecturer at the Department of Physics at Andalas University in Indonesian. She is also currently taking part in a doctoral program in materials physics at Bandung Institute of Technology, in Indonesia. She obtained her master degree in Physics at the Bandung Institute of Technology (2015). She is interested in researching materials physics, including the thermal properties of materials and materials synthesis. Research into the thermal properties of materials is focused on studying the energy conversion contained in material phase changes. Meanwhile, research topics in material synthesis are focused on the synthesis of luminescent nanoparticles.